

# Arabidopsis MRG domain proteins bridge two histone modifications to elevate expression of flowering genes

Yifeng Xu<sup>1</sup>, Eng-Seng Gan<sup>1,2</sup>, Jie Zhou<sup>1</sup>, Wan-Yi Wee<sup>1</sup>, Xiaoyu Zhang<sup>3</sup> and Toshiro Ito<sup>1,2,\*</sup>

<sup>1</sup>Temasek Life Sciences Laboratory, National University of Singapore, Singapore 117604, Republic of Singapore,

<sup>2</sup>Department of Biological Sciences, National University of Singapore, Singapore 117543, Republic of Singapore and

<sup>3</sup>Department of Plant Biology, University of Georgia, Athens, GA 30602-7271, USA

Received April 14, 2014; Revised July 30, 2014; Accepted August 18, 2014

## ABSTRACT

Trimethylation of lysine 36 of histone H3 (H3K36me3) is found to be associated with various transcription events. In *Arabidopsis*, the H3K36me3 level peaks in the first half of coding regions, which is in contrast to the 3'-end enrichment in animals. The MRG15 family proteins function as 'reader' proteins by binding to H3K36me3 to control alternative splicing or prevent spurious intragenic transcription in animals. Here, we demonstrate that two closely related *Arabidopsis* homologues (MRG1 and MRG2) are localised to the euchromatin and redundantly ensure the increased transcriptional levels of two flowering time genes with opposing functions, *FLOWERING LOCUS C* and *FLOWERING LOCUS T (FT)*. MRG2 directly binds to the *FT* locus and elevates the expression in an H3K36me3-dependent manner. MRG1/2 binds to H3K36me3 with their chromodomain and interact with the histone H4-specific acetyltransferases (HAM1 and HAM2) to achieve a high expression level through active histone acetylation at the promoter and 5' regions of target loci. Together, this study presents a mechanistic link between H3K36me3 and histone H4 acetylation. Our data also indicate that the biological functions of MRG1/2 have diversified from their animal homologues during evolution, yet they still maintain their conserved H3K36me3-binding molecular function.

## INTRODUCTION

In eukaryotes, including plants, post-translational covalent modifications on histones play a pivotal role in controlling gene expression at the chromatin level. Different histone modifications act sequentially or in combination to confer distinct transcriptional outcomes. Although histone modifications are conserved to a large extent amongst eukaryotes, there is some divergence in terms of the distribution

of these histone modifications in the genome and their biological functions between plants and animals. For example, in yeast, worms and mammals, trimethylation of lysine 36 of histone H3 (H3K36me3) preferentially marks the exons of transcribed genes and peaks at the 3'-end of the coding region, and it has been shown to be involved in various activities, including the control of alternative splicing and the prevention of spurious intragenic transcription (1–5). In contrast, the H3K36me3 level in *Arabidopsis* peaks at the 5'-end of the coding region, which resembles the distribution patterns of active transcription-linked histone modifications, H3K4me2/3 and acetylated H3 (6). This preferential enrichment at the first half of the coding region in plants suggests that the mechanism governing H3K36me3 deposition, and possibly its effect on transcriptional events, may differ between plants and other eukaryotes.

Whilst some histone modifications such as acetylation can directly modulate chromatin structures, an increasing body of evidence suggests that individual histone modifications, or a combination of them, may serve as a platform to recruit specific 'reader' proteins, which then determine the transcriptional outcome of the target genes. The yeast homologue of the human MORF4-related gene on chromosome 15 (MRG15), Esa1-associated factor 3 (Eaf3), was the first identified 'reader' for H3K36me3 (2–4). MRG15 proteins are highly conserved across multiple species, including fruit flies (*Drosophila melanogaster*), worms (*Caenorhabditis elegans*) and yeast (*Schizosaccharomyces pombe* and *Saccharomyces cerevisiae*) (7,8). The MRG15 family proteins contain the conserved chromodomain at its amino terminus, which binds to H3K36me3. Chromodomain and chromo-like domain (such as Tudor and PWWP domains) are protein modules that are found in many chromatin-related proteins in nucleoprotein complexes (9). They have been shown to recognise and bind to methylated-Lys at the histone tails and hence recruit the protein complexes to play an important role in histone modifications and chromatin-remodelling, which control the transcription status of a large number of genes. For example, the chromodomain of chromatin-binding proteins heterochromatin-binding protein 1 (HP1) and Polycomb (Pc) bind to methylated Lys9

\*To whom correspondence should be addressed. Tel: +65 6872 7016; Fax: +65 6872 7007; Email: itot@tll.org.sg

and Lys27 of histone H3, respectively, directing heterochromatin formation and/or gene silencing (10–13). The chromodomain of human MRG15 and its homologue in yeast, Eaf3, which is unlike the typical chromodomain found in HP1 and Pc proteins, is assumed to be an auto-inhibited chromo barrel domain and binds to trimethylated H3K36 and H3K4 *in vitro* with a relatively weak affinity (2–4,14–16).

In addition to the chromodomain, all members of the MRG family proteins contain the MRG domain, which shares sequence similarity with the Mortality factor on chromosome 4 (MORF4), a cell-senescence protein in humans, and that may be involved in protein–protein interactions (2–4,8,17,18). Biochemical assays have shown that the animal MRG15 proteins and the yeast homologues associate with at least two independent and antagonising nucleoprotein complexes that contain either histone acetyltransferases (HAT) or histone deacetylases (HDAC) (2–4,18–20). In mouse and *Drosophila*, deletion or knockdown of *MRG15* genes cause embryonic-lethal phenotypes, whilst loss-of-function of *S. cerevisiae* Eaf3 and *S. pombe* Altered polarity mutant-13 (Alp13) are viable (21,22). The loss of *Alp13* in fission yeast causes growth arrest, sterility, defects in cell polarity and is associated with global hyperacetylation of histones and chromosome instability (22). Alp13 represses the expression of repeated regions and maintains the heterochromatin through the recruitment of histone deacetylation complexes to the repeat regions (23). Eaf3 in *S. cerevisiae* was suggested to suppress intragenic transcriptional initiation by recruiting the histone deacetylase complex to H3K36me3-containing nucleosomes (2–4). Eaf3 also specifically targets promoter regions of heat-shock and ribosomal protein genes for transcriptional activation through the recruitment of NuA4-dependent histone H4 acetylation complexes (24–26). Due to these dual functions, the deletion of *Eaf3* greatly alters the global genomic profile of histone modification, with increased acetylation levels at coding sequences and decreased acetylation levels at the promoter regions (21). *MRG-1*, an *MRG15* homologue in *C. elegans*, was recently reported to be involved in homologous chromosome pairing, which is independent of both the pairing centre and meiotic homologous recombination (27). These data suggest that the function of MRG15 family proteins have diversified in different species and participate in varied biological processes. The *Arabidopsis* genome contains two *MRG15* homologues with high similarities in their protein sequences (8). However, whether they maintain their functions as H3K36me3 readers and effectors and which biological process they are involved in are largely unknown.

Histone acetylation is one of the histone modifications that is well known to be linked with active transcription (28). Histone acetylation may neutralise a positive charge and thus weaken the interaction of the histone octamer with the negatively charged DNA and/or interfere with the higher-order packing of chromatin, which allow transcriptional regulators to gain access to the DNA with a larger chromatin area (28). Different families of HATs have distinct histone targets and are involved in different biological events (28). One well-studied family of the acetyltransferases responsible for histone acetylation is the MYST

(for MOZ, Ybf2/Sas3, Sas2 and Tip60)-related HATs (29). MYST proteins contain the acetyl-CoA binding motif as well as a C2HC zinc finger motif that is important for HAT activity and interact with the MRG15 family proteins (18,20,29). The yeast MYST HAT Esa1 associates with the MRG15 protein Eaf3 to specifically target promoter regions of heat-shock and ribosomal protein genes for transcriptional activation (20,24–26). Thus, the substrate specificity of the MYST protein is likely conferred through association with additional complex subunits. The *Drosophila* HAT, MOF, associates with the MRG protein, MSL3, in a mutually dependent manner to target Histone H4 in the X-chromosome dosage compensation mechanism and autosomal transcription regulation (30,31). In *Arabidopsis*, there are two functionally redundant MYST family proteins, namely, HISTONE ACETYLTRANSFERASE OF THE MYST FAMILY 1 (HAM1) and HAM2 (32). HAM1 and HAM2 have HAT activity specific to H4K5 *in vitro* and *in vivo* (33,34). The double-mutant *ham1 ham2* is not viable, and mutation of either *ham1* or *ham2* did not show any defects in vegetative and reproductive stages (32). Interestingly, *ham1/+ ham2/+* plants showed a reduction in the *FLOWERING LOCUS C* (*FLC*) expression level, with a reduction of H4K5 acetylation at the *FLC* locus (32,34), suggesting that HAM1 and HAM2 have essential functions in various developmental processes, including flowering control.

Flowering is a highly regulated biological process in *Arabidopsis*. At the centre of the flowering control is the floral repressor *FLC*, which integrates multiple inputs from different flowering pathways and functions to repress two downstream floral inducers, *FLOWERING LOCUS T* (*FT*) and *SUPPRESSOR OF OVEREXPRESSION OF CONSTANS 1* (*SOC1*). *FLC* expression is governed by multiple epigenetic regulators (35). The H3K36me3 marks have an active effect on the transcription of *FLC*, and the loss-of-function mutant of the H3K36-methyltransferase SET DOMAIN GROUP 8 (SDG8), a homologue of the yeast histone H3K36-methyltransferase *SET2*, causes a drastic decrease in the *FLC* expression (36–38). However, the exact mechanistic function of SDG8-mediated H3K36me3 on *FLC* expression is largely unknown. In this study, we show that MRG1 and MRG2 function redundantly as the H3K36me3 ‘reader’ and ‘effector’ in the fine-tuning of transcription of flowering time genes *FLC* and *FT*. MRG1 and MRG2 bind to their targets and recruit histone acetyltransferase HAM1 and HAM2 complex to increase the histone H4 acetylation levels on the target loci, thereby making these loci more accessible to transcriptional machinery, hence bridging H3K36 methylation and histone H4 acetylation.

## MATERIALS AND METHODS

### Plant materials and growth conditions

All *Arabidopsis thaliana* plants used were in the background of the Columbia (Col) ecotype. The alleles of *mrg1-1* (SAIK\_057762), *mrg2-1* (SALK\_035089), *mrg2-2* (SK28487) and *mrg2-3* (GK-255G06) were isolated from the SALK, SK and GABI-Kat collections, respectively. The *sdg8* allele (*sdg8-2*) was described previously (38). The allele

of *sdg7* (SALK\_131218) in which T-DNA is inserted in the exon 4 were isolated from SALK collections. Plants were grown in LDs (16-h light/8-h dark) at 23°C. Genotyping primer sequences are shown in Supplementary Table S1.

### Plasmid construction and plant transformation

To construct *35S::MRG2-HA* and *35S::GFP-MRG2* plasmids, the full length *MRG2* coding sequence was amplified by primer set MRG2-MluI\_F and MRG2-XmaI\_R1, or MRG2-ApaI\_F and MRG2-XmaI\_R2, cloned into vectors *pGREEN-35S-HA* by using *MluI* and *XmaI* or *pGREEN-35S-GFP* by using *ApaI* and *XmaI*.

For *pMRG2::MRG2-GUS*, *pMRG2::HA-MRG2* and *pHAM1::HA-HAM1* plasmids, a ~7.2-kb *MRG2* genomic fragment (from -3406 to +3845; A of the start codon was set as +1) and a ~4.0-kb *HAM1* genomic fragment (from -1371 to +2579) amplified using primers gDMRG2-cacc\_F and gDMRG2-XmaI\_R or gDHAM1-cacc\_F and gDHAM1\_R were cloned into *pENTR/D-TOPO* vector (Invitrogen). *SfoI* restriction site was introduced after ATG or in front of the *MRG2* stop codon, or after ATG of *HAM1* through mutagenesis using primers mMRG2-ATG-SfoI\_F and mMRG2-ATG-SfoI\_R, mMRG2-Stop-SfoI\_F and mMRG2-Stop-SfoI\_R, or mHAM1-ATG-SfoI\_F and mHAM1-ATG-SfoI\_R, respectively. *HA* or *GUS* fragments were then inserted into the *SfoI* site of the *pENTR/D-TOPO-gDMRG2* or *pENTR/D-TOPO-gDHAM1* plasmid. Finally, *gDMRG2-GUS*, *HA-gDMRG2* or *HA-gDHAM1* in *pENTR/D-TOPO* plasmids were recombined into *pBGW* or *pHGW* using LR Clonase II (Invitrogen), respectively.

For *pMRG1::MRG1-GUS* plasmid, a ~3.2-kb *MRG1* genomic fragment (from -321 to +2878) spanning to the neighbouring genes located to the upstream and downstream of *MRG1* was cloned into *Topo-PCR II* (Invitrogen) first using the primer set gDMRG1-NotI\_F and gDMRG1\_R. The genomic fragment was then released with *NotI* digestion and cloned into the modified *pENTR* vector. Mutagenesis was performed using the primers mMRG1-Stop-ScaI\_F and mMRG1-Stop-ScaI\_R. The *GUS* fragment was then inserted into the *ScaI* site of the *pENTR-gDMRG1* plasmid. Finally, *MRG1* in *pENTR* was recombined into *pBGW* using LR Clonase II (Invitrogen). All the vectors were verified by sequencing. Primer sequences are listed in Supplementary Table S1.

Transgenic plants were generated by floral dipping with *Agrobacterium tumefaciens* with the corresponding constructs. The additional *pSOUP* helper plasmid was co-transfected for the transformation of *pGREEN-35S::MRG2-HA* and *pGREEN-35S::GFP-MRG2*.

### RNA extraction and expression analysis

For the tissue expression analysis of *MRG1* and *MRG2*, total RNAs were isolated from the root, juvenile rosette leaf, mature rosette leaf, cauline leaf, stem, flower bud, open flower and silique. For the flowering time gene expression analysis, the aerial parts of 6 day-after-germination (DAG) and 9 DAG seedlings were harvested at dusk (ZT16). For a time course assay over a 24-h-long day cycle, the aerial

parts of 9 DAG seedlings were harvested every 2 or 4 h. The total RNAs were extracted using an RNeasy plant mini kit (Qiagen) according to the manufacturer's instructions. Approximately 500 ng total RNAs were used for reverse transcription with the Superscript III RT-PCR system (Invitrogen). Semi-quantitative PCR (semi-qPCR) with gene-specific primers (Supplementary Table S1) were performed using HotStarTaq DNA Polymerase (Qiagen) on a Thermocycler (Bio-Rad) at 25–35 cycles. Real-time qPCR was performed on ABI PRISM 7900HT sequence detection system (Applied Biosystems) using KAPA SYBR FAST ABI Prism qPCR Master Mix (KAPA Biosystems). The ubiquitously expressed *Tip41-like* (AT4G34270) (39) was used as an internal reference gene. Primer sequences were shown in Supplementary Table S1.

### GUS staining

GUS staining was performed as previously described (40). Briefly, plant tissues were fixed with ice-cold 90% acetone for 30 min and rinsed with rinsing solution. The tissues were then incubated in staining solution at 37°C for approximately 8 h. After staining, the tissues were incubated in fixation solution overnight and washed with a serial of ethanol solution. For histological analysis, the tissues were mounted on slides with clearing solution, and images were taken with an AxioCam ICc 3 (Zeiss) under a SteREO Discovery.V12 Stereomicroscope (Zeiss).

### Chromatin immunoprecipitation (ChIP) assays

ChIP experiments were performed as previously described with minor modifications (41). Briefly, total chromatin was extracted from 10 DAG seedlings and immuno-precipitated using anti-HA (Santa Cruz Biotechnology, #sc-7392) and normal mouse IgG as a control (Santa Cruz Biotechnology, #sc-2025), or anti-H3Ace3 (Millipore, #06-599), anti-H4K5Ace (Active Motif #39699), anti-H3K4me3 (Active Motif #61379) and anti-H3K36me3 (Active Motif #61021), with anti-H3 (Abcam, #ab1791) as a control. DNA fragments were recovered by phenol-chloroform extraction and ethanol precipitation. Quantitative PCR with locus-specific primers (Supplementary Table S1) was performed to measure the amounts of *FT* relative to that of the constitutively expressed *ACTIN2* (AT3G18780) on ABI PRISM 7900HT sequence detection system (Applied Biosystems) using KAPA SYBR FAST ABI Prism qPCR Master Mix (KAPA Biosystems).

### Bimolecular fluorescence complementation (BiFC) assay

The full-length coding sequences for *MRG1*, *MRG2*, *HAM1* and *HAM2* were fused in frame with either the coding sequence for an N-terminal yellow fluorescent protein (YFP) fragment or for a C-terminal YFP fragment in the primary pSAT1 vectors (42). To detect the interaction in tobacco, leaves of 2- to 4-week-old tobacco plants were infiltrated with *Agrobacterium* containing the respective plasmid pairs (43). Epidermal cell layers were examined 2–4 days after infiltration and imaged with a Zeiss LSM 5 EXCITER upright laser scanning confocal microscope (Zeiss) (41).

### Co-immunoprecipitation (Co-IP) assays

Co-IP experiments were performed as described previously with minor modifications (41). Briefly, 10-day-old seedlings (~2 g) expressing *pHAM1::HA-HAM1 35S::GFP-MRG2* or *pHAM1::HA-HAM1* were harvested and total proteins were extracted and immunoprecipitated with anti-GFP antibody (Invitrogen, #A-11122). The HA-HAM1 protein in the immunoprecipitates was detected by western blotting with anti-HA-HRP (Santa Cruz Biotechnology, #sc-7392).

### Immunostaining and *in situ* proximity ligation assay

Isolation of nuclei and *in situ* immunolocalisation of chromatin proteins were performed as described with minor modifications (44). Young leaves from *sdg8*, *sdg7 sdg8*, wild-type or *pMRG2::HA-MRG2* transgenic plants were used for nuclei extraction. Sample suspension was air-dried on glass slides. Each slide was blocked with 1% BSA in 1x PBS before incubating with mouse anti-H3K36me3 (Active Motif #61021) and rabbit anti-H3K36me2 (Abcam, #ab9049), or with rabbit anti-HAM1/2 (Aviva, #ARP33345.P050) and mouse anti-HA (Santa Cruz Biotechnology, #sc-7392), rabbit anti-H3K36me3 (Abcam, #ab9050) and mouse anti-H3K4me3 (Active Motif #61379), and rabbit anti-H3K9me2 (Abcam, #ab1220). Later the slides were incubated with CF555 goat anti-mouse IgG (Biotium, #20030) and/or CF 488A goat anti-rabbit IgG (Biotium, #20010). Slides were stained with DAPI and imaged with Leica TCS SP5 confocal microscope (Leica).

The *in situ* proximity ligation assay (PLA) assay was carried out with Duolink II kits (Genome holdings) according to the manufacturer's instructions, with nuclei prepared with *pMRG2::HA-MRG2* transgenic plants, wild-type plants and *pMRG2::MRG2-HA* in a *sdg8* background, in a way similar to the *in situ* immunolocalisation assay. Mouse anti-HA (Santa Cruz Biotechnology, #sc-7392) and rabbit anti-H3K4me3 (Millipore, #07-473), rabbit anti-H3K36me3 (Abcam, #ab9050), rabbit anti-H3 (Abcam, #ab1791), rabbit anti-HAM1/2 (Aviva, #ARP33345.P050), rabbit anti-H3K9me2 (Abcam, #ab1220) or rabbit IgG (Santa Cruz, #SC-2027) were used as the primary antibodies. After washing, Duolink II PLA Probe anti-Mouse Plus (Genome holdings, #92001-0030) and Duolink II PLA Probe anti-Rabbit Minus (Genome holdings, #92005-0030) were applied as the probes. Duolink II Detection Reagents (Genome holdings, #92008-0030) were used to amplify the interaction signal, and the fluorescent signal was imaged with a Leica TCS SP5 confocal microscope (Leica).

### Peptide pull-down assays

The chromodomain of MRG1 (1-131 aa) or MRG2 (1-130 aa) was cloned into *pGST-4T-1* (GE Healthcare) with the primer set GST-MRG1-CD-BamHI.F and GST-MRG1-CD-XmaI.R, or GST-MRG2-CD-BamHI.F and GST-MRG2-CD-XmaI.R. GST alone, GST-MRG1 CD or GST-MRG2 CD (1 µg) expressed in *E. coli* Rosetta was incubated in binding buffer [20 mM Tris-HCl pH 8.0, 250 mM NaCl, 1 mM EDTA, 0.5% NP-40, 1 mM

phenylmethylsulfonyl fluoride, 1 mM DTT, 1x protease inhibitor cocktail (Roche)] with 10 µg of BSA and 1 µg biotinylated trimethylated histone H3K36 peptide (Epigentek, #R-1050-100), trimethyl histone H3K4 (Epigentek, #R-1023-100), trimethyl histone H3K9 (Epigentek, #R-1029-100), trimethyl histone H3K27 (Epigentek, #R-1035-100) or biotinylated unmodified histone H3 aa 22-44 (Epigentek, #R-1006-100) and biotinylated unmodified histone H3 aa 1-21 (Epigentek, #R-1004-100) immobilised on streptavidin-agarose. The beads were then washed with binding buffer and analysed by western blotting with antibodies against GST (Santa Cruz, #sc-138).

## RESULTS

### The *mrg1 mrg2* double mutant shows a late-flowering phenotype

In *Arabidopsis*, there are two closely related *MRG15* homologues *MRG1* (AT4G37280) and *MRG2* (AT1G02740) that share high sequence similarities (Supplementary Figure S1; (8)). We first identified the *mrg2-1* (SALK\_035089) mutant, in which the T-DNA insertion in the fourth exon (Figure 1A) abolished the expression of the full-length transcript of *MRG2* (Figure 1B). Whilst the homozygous plants showed male and female sterility due to a meiosis defect, fertility was normal in other *mrg2* loss-of-function alleles, indicating that it is not linked with the *mrg2* mutation. We also identified the *mrg1-1* (SALK\_057762) mutant, in which T-DNA is inserted in the first intron with no full-length transcript produced (Figure 1A and B). Although the single *mrg1-1* did not show any mutant phenotypes, *mrg1-1 mrg2-1* showed a late-flowering phenotype under long-day (LD) growth conditions (Figure 1C, Supplementary Figure S2A and B). We isolated two more T-DNA mutant alleles of *mrg2*, *mrg2-2* (SK28487) and *mrg2-3* (GK-255G06) (Figure 1A). T-DNA insertion in the first and ninth intron, respectively, abolished the production of the *MRG2* full-length transcript (Figure 1A and B, Supplementary Figure S2A, E), but they did not show any sterility phenotype. Consistent with *mrg1-1 mrg2-1*, *mrg1-1 mrg2-2* and *mrg1-1 mrg2-3* showed similar late-flowering phenotypes (Figure 1C and D, Supplementary Figure S2A-D). Moreover, introduction of the *pMRG2::HA-MRG2* transgene into *mrg1-1 mrg2-2* completely rescue the late-flowering phenotype in the *mrg1 mrg2* double mutant (Figure 1C and D). These results show that MRG1 and MRG2 are redundantly involved in flowering control. Due to the similarity in their phenotype, we used *mrg1-1 mrg2-2* (herein *mrg1 mrg2*) for all subsequent experiments.

### MRG1 and MRG2 are required for higher expression levels of *FLC* and *FT*

To investigate which flowering genes are responsible for the late-flowering phenotype in *mrg1 mrg2*, we harvested the aerial parts of the seedlings at 9 DAG (day after germination, at the beginning of the dark photoperiod under LD conditions) just before the floral induction. We then compared the expression of a series of flowering time genes between WT and *mrg1 mrg2*. Whilst *AGL24*, *MAF1-5* and *SVP* were un-affected in *mrg1 mrg2* (Supplementary Figure

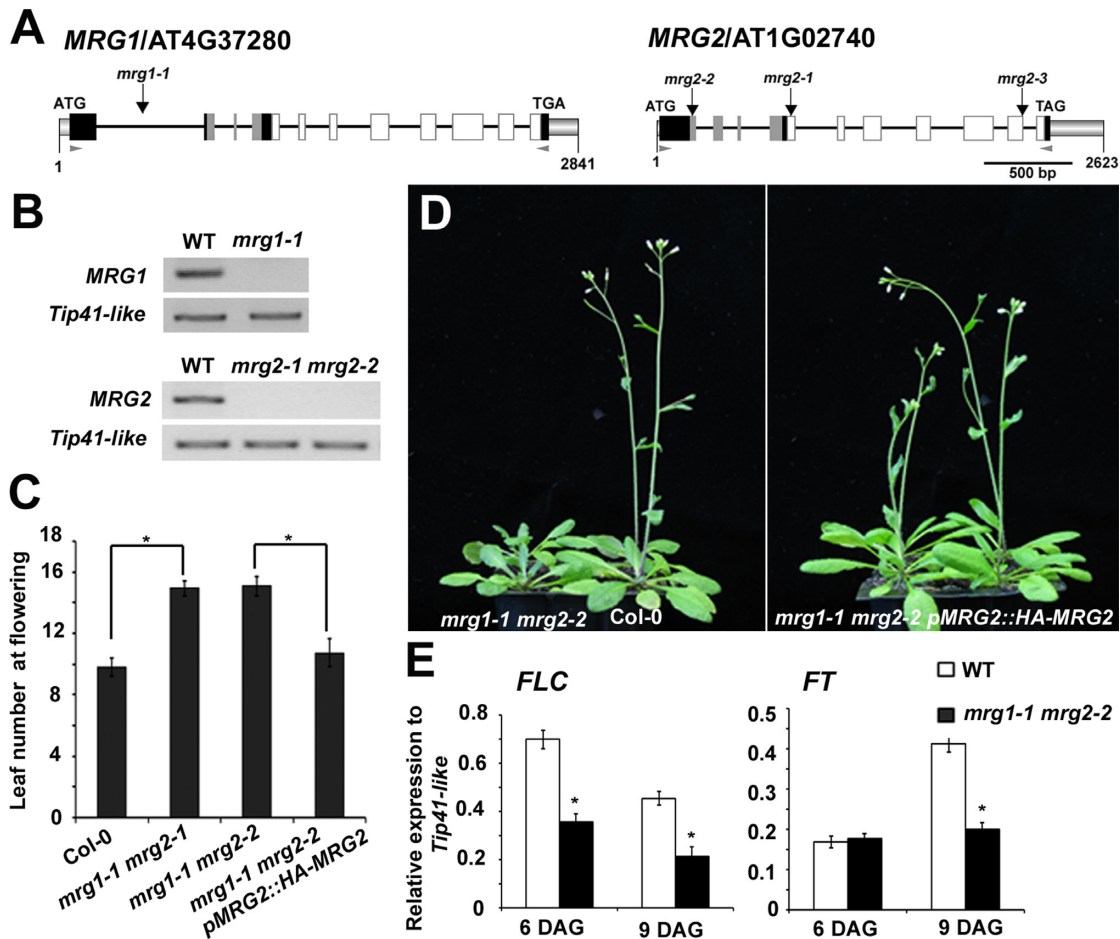


**Figure 1.** *MRG1* and *MRG2* are required for high transcriptional levels of *FT* and *FLC*. (A) Schematic drawings of the genomic structures of *MRG1* and *MRG2*. The smaller gray boxes indicate the 5' and 3' UTRs. Black lines indicate the introns. The larger boxes indicate exons with gray boxes and white boxes further showing the chromodomain and MRG domain coding regions, respectively. T-DNA insertion sites are marked by downward arrows above the schematic diagrams. The pairs of arrowheads on *MRG1* and *MRG2* genomic structures indicate the position for the semi-quantitative RT-PCR primers designed to detect *MRG1* and *MRG2* transcripts. Bar, 500 bp. (B) Semi-quantitative RT-PCR of *MRG1* and *MRG2* in Col wild-type (WT), *mrg1-1*, *mrg2-1* and *mrg2-2*, respectively. Primers are shown in A. Ubiquitously expressed *Tip41-like* gene (AT4G34270) was used as a control. (C) Total number of rosette leaves before bolting in Col WT, *mrg1-1 mrg2-1*, *mrg1-1 mrg2-2* and *mrg1-1 mrg2-2 pMRG2::HA-MRG2* plants grown in 16 h light/8 h dark long-day condition (LD) at 23°C were counted (two independent experiments with 15–20 plants each). \**P* < 0.05 with Student's *t*-test to indicate the difference of flowering time between Col WT and *mrg1-1 mrg2-1*, *mrg1-1 mrg2-2* and *mrg1-1 mrg2-2 pMRG2::HA-MRG2*. No significant difference between *mrg1-1 mrg2-2* and *mrg1-1 mrg2-3* (*P* = 0.50), Col WT and *mrg1-1 mrg2-2 pMRG2::HA-MRG2* (*P* = 0.49). (D) *mrg1-1 mrg2-2* bolted later than Col WT when grown in LD 23°C (2 plants each, left panel), and *pMRG2::HA-MRG2* rescued the late-flowering phenotype of *mrg1-1 mrg2-2* (right panel) grown at the same condition. (E) Quantitative RT-PCR-based expression levels of *FLC* and *FT* in 6 and 9 DAG seedlings of Col WT and *mrg1-1 mrg2-2* grown in LD 23°C. Bars indicate SD of three biological replicates. \**P* < 0.05 with Student's *t*-test.

S3A–G), *FLC*, *FT* and *SOCI* transcription levels were reduced approximately 2-fold in *mrg1 mrg2* (Figure 1E, Supplementary Figure S3H). As *SOCI* is one of the downstream targets of FT, the reduction of *SOCI* could be due to the indirect effect of loss-of-function of *mrg1* and *mrg2*. Because FT functions downstream of *FLC*, the *FT* reduction at 9 DAG may lead to late-flowering. Down-regulation of *FT* in spite of the reduced *FLC* expression in the mutant indicates that *FT* may be directly controlled by *MRG1* and *MRG2*. To further characterise the transcriptional change of *FLC* and *FT* in *mrg1 mrg2*, we next compared their expression between WT and *mrg1 mrg2* plants at an earlier stage at 6 DAG, and found that *FLC* expression is reduced to half in *mrg1 mrg2* at both 6 DAG and 9 DAG (Figure 1E). Although *FT* showed a 2-fold decrease in expression at 9

DAG, the *FT* expression at 6 DAG was not affected (Figure 1E). *FT* is expressed at a relatively low level in the WT plant at 6 DAG compared with that at 9 DAG (45). Similar expression patterns of *FT* and *FLC* were also observed in the different allele *mrg1-1 mrg2-3* (Supplementary Figure S2F). These data suggest that two redundant *MRG1* and *MRG2* are essential in ensuring the maximum endogenous expression level of their putative targets *FT* and *FLC* but may not act in the initial transcriptional activation of *FT*. Transcriptional up-regulation by *MRG1* and *MRG2* on *FT* may require a threshold level of *FT* expression or the accumulation of the transcription-associated epigenetic marks, such as H3K36me3.

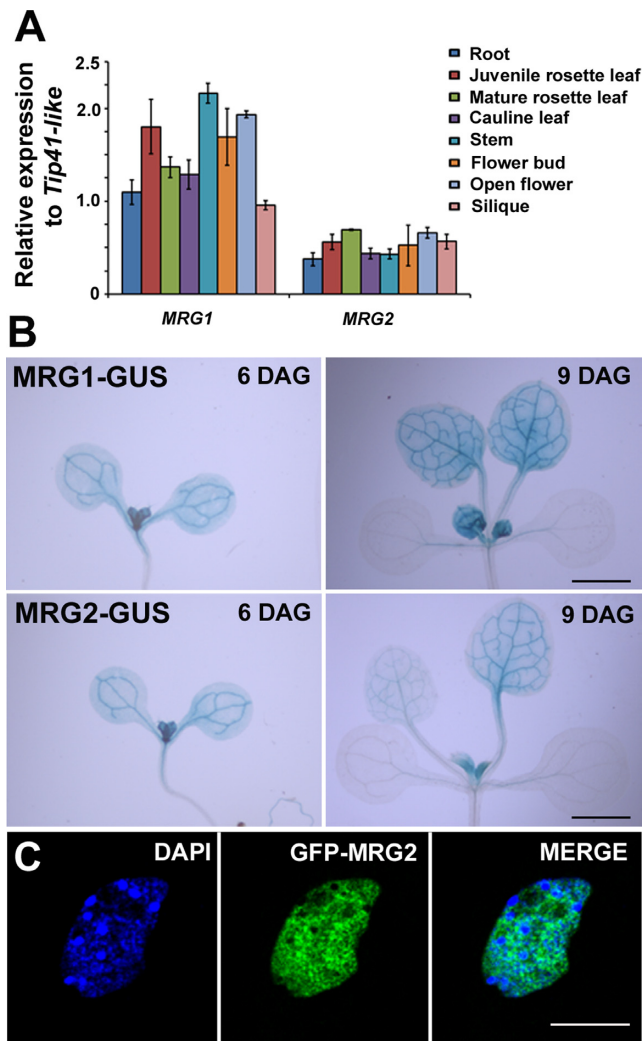


**Figure 2.** MRG1 and MRG2 are ubiquitously expressed and localised in euchromatin. (A) RT-qPCR-based expression levels of *MRG1* and *MRG2* in different tissues, including root, juvenile rosette leaf, mature rosette leaf, cauline leaf, stem, flower bud, open flower and silique. (B) Histochemical GUS staining of *pMRG1::MRG1-GUS* and *pMRG2::MRG2-GUS*. Seedlings at 6 and 9 DAG were stained for 8 h. Scale bar, 2 mm. (C) Immunolocalisation of GFP-MRG2 in the nuclei of a root cell of *35S::GFP-MRG2* transgenic line. Scale bar, 10  $\mu$ m.

### MRG1 and MRG2 are localised at euchromatin

Quantitative RT-PCR with RNA extracted from different tissues showed that *MRG1* and *MRG2* are ubiquitously expressed in the whole plants (Figure 2A). A GUS staining assay of plants harbouring the GUS fusion transgene *pMRG1::MRG1-GUS* and *pMRG2::MRG2-GUS* confirmed that *MRG1* and *MRG2* expression is detectable in all tissue types, especially in the vasculatures of true leaves and young leaf primordia (Figure 2B), which match the expression patterns of *FLC* and *FT*. The sub-cellular localisation of the MRG proteins was examined using the root of *35S::GFP-MRG2* transgenic plants. GFP-MRG2 was found to be localised in the euchromatic regions of the nucleus but not in the DAPI-dense heterochromatin

(Figure 2C), consistent with the previous reports that MRG proteins function as chromatin remodelling factors (8).

### MRG2 binds to H3K36me3 *in vitro* and *in vivo*

It has been shown that the chromodomain at the N-terminus of MRG15 homologues can bind to H3K36me3 in both yeast and humans and to H3K4me3 in yeast with low affinity (2–4,14–16). To check whether the chromodomain of *Arabidopsis* MRG proteins interacts directly with these modified histones, we cloned the N-terminal chromodomain (1–131 aa) of MRG1 and chromodomain (1–130 aa) of MRG2 to produce the GST-MRG1/2 chromodomain fusion proteins (MRG1-CD and MRG2-CD in Figure 3A) and performed a pull-down assay using different histone H3 peptides trimethylated at K4, K9, K27, K36, dimethylated at K36 or two unmodified histone H3 peptides (H3 1–21 and H3 21–44), all of which were biotin-labelled and immobilised on streptavidin agarose beads. Both of the chromodomains of MRG1 and MRG2 were found to bind to H3K36me2, H3K36me3 and H3K4me3 with different affinities, but not to the other histone modifications (H3K9me3 and H3K27me3) nor the unmodified histone H3 (Figure 3A). Thus, the histone-binding function of MRG1/2 to H3K36me2/3 is rather conserved across different species, but like the yeast homologue, they also bind to H3K4me3.

An *in situ* PLA provides another piece of evidence to support the model that MRG2 binding to histone H3 is mediated through H3K36me3 and/or H3K4me3 *in vivo*. An *in situ* PLA is able to detect the direct protein interaction with high sensitivity and specificity by integrating traditional immunolocalisation techniques with DNA-based signal amplification (46). We first carried out the immunofluorescence staining with antibody against HA-MRG2, MYST family HATs HAM1/2, H3K36me3 and H3K9me2, and confirmed that HA-MRG2 and HAM1/2 are co-localised at the euchromatin (Supplementary Figure S4C) in a similar pattern with the euchromatic histone modifications H3K4me3 and H3K36me3 (Supplementary Figure S4B), whilst H3K9me2 is specifically detectable at the heterochromatin region (Supplementary Figure S4A). Next, we performed *in situ* PLA assay with the tested antibodies. Using antibodies against HA and H3K4me3 and H3K36me3, the fluorescence signals of PLA were detected in the nuclei harvested from *pMRG2::HA-MRG2* plants but not in WT plants without the transgene (Figure 3B and C). The negative control, using an H3K9me2 antibody, showed there is no interaction between H3K9me2 and HA-MRG2 in transgenic plants. These results indicate the close localisation between MRG2 with H3K4me3 and H3K36me3 *in vivo* (Figure 3C).

### MRG proteins function through SDG8-mediated H3K36me3

Immunostaining using the nuclei of wild-type and *sdg8* mutant leaf cells showed that mutation of the *Arabidopsis* H3K36 methyltransferase *SDG8* leads to a near complete abolishment of H3K36me3 and a slight reduction in H3K36me2 (Figure 4A) (37,38). The double mutant with another close homologue of *SDG8*, *sdg7 sdg8* fully abol-

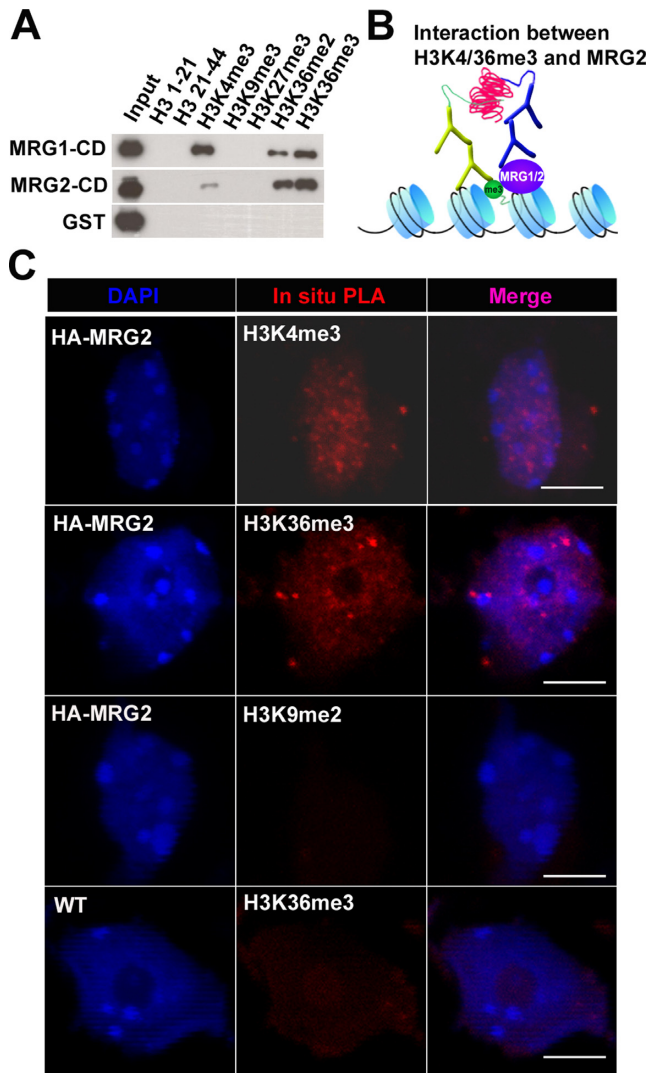


**Figure 3.** MRG2 directly binds to H3K36me3 *in vitro* and *in vivo*. (A) *In vitro* binding assay. Bacteria-expressed GST alone or GST-MRG1/2 chromodomains (MRG1-CD and MRG2-CD) were tested for binding to biotinylated unmodified histone H3 (H3 1–21 amino acid and H3 21–44 amino acid) or modified histone H3K4me3, H3K9me2, H3K27me3, H3K36me2 and H3K36me3 peptides immobilised on streptavidin-agarose. MRG1/2-CD were pulled down only by H3K4me3 and H3K36me2/3. GST was used as the negative control. (B) Schematic diagram showing *in situ* PLA assay between MRG2 and H3K4/36me3. (C) *In situ* PLA assay performed using anti-HA and anti-H3K4me3/H3K36me3 antibodies to show the interaction between HA-MRG2 and H3K4me3/H3K36me3. Blue, DAPI. Red, *in situ* PLA signals showing the interaction between HA-MRG2 and H3K4me3/H3K36me3. Purple, merge. Top two rows, *in situ* PLA assay using anti-HA and anti-H3K4me3/H3K36me3 antibodies in *pMRG2::HA-MRG2*; third row, *in situ* PLA assay between *pMRG2::HA-MRG2* and H3K9me2 as a negative control; bottom row, *in situ* PLA assay using anti-HA and anti-H3K36me3 antibodies in WT as a negative control. Scale bar, 5  $\mu$ m.

ishes both the di- and tri-methylation marks at H3K36 (Figure 4A). In *sdg8* and *sdg7 sdg8*, *FLC* expression is almost fully abolished, suggesting that the H3K36me3 is essential for *FLC* expression (Figure 4B) (37). We found that H3K36me2, as in *Drosophila*, may function differently from H3K36me3 in *Arabidopsis*, because detectable, albeit dras-

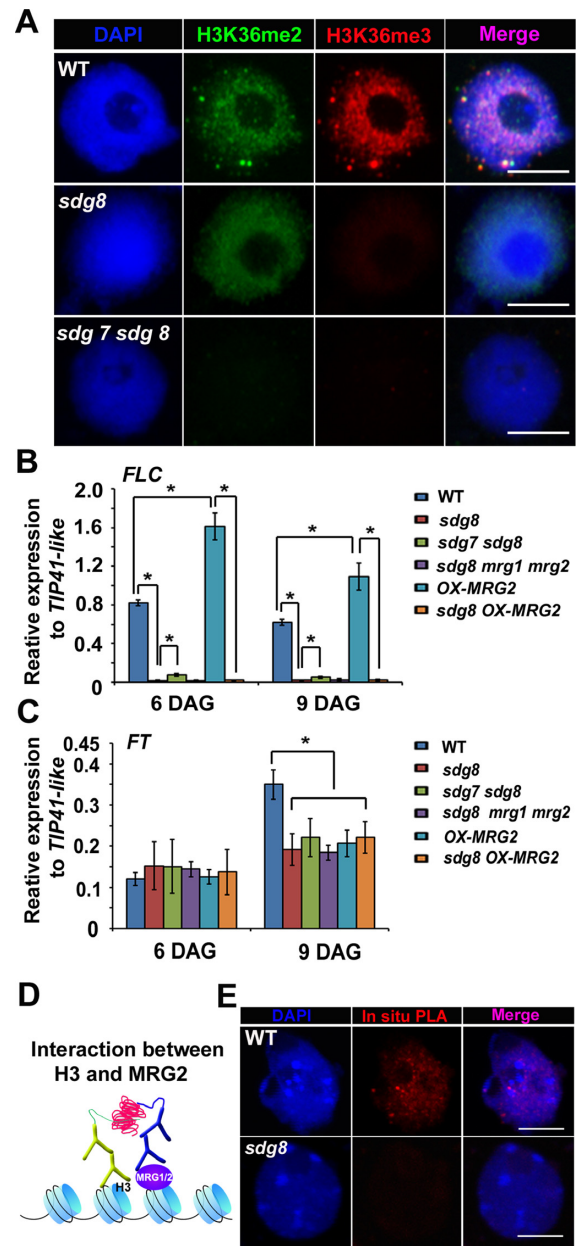


**Figure 4.** MRG1/2 function is dependent on H3K36me3. (A) Dual immunolocalisation of H3K36me2 and H3K36me3 in Col wild-type (WT, top panels), *sdg8* (middle panels) and *sdg7 sdg8* (bottom panels) nuclei. H3K36me2 (green) and H3K36me3 (red) were detectable using the respective antibodies in WT but not in *sdg7 sdg8*, whilst *sdg8* could still retain a reduced level of H3K36me2. Blue, DAPI. Scale bar, 5  $\mu$ m. (B–C) RT-qPCR of *FLC* (B) and *FT* (C) expression in Col WT, *sdg8*, *sdg7 sdg8*, *sdg8 mrg1 mrg2*, *35S::MRG2-HA (OX-MRG2)* and *sdg8 OX-MRG2*. Error bars indicate SD of three biological replicates. \* $P < 0.05$  between *FLC* expression in Col WT and *sdg8*, *sdg8* and *sdg7 sdg8*, *OX-MRG2* and *sdg8 OX-MRG2*, Col WT and *OX-MRG2* at both 6 DAG and 9 DAG with Student's *t*-test. \* $P < 0.05$  between *FT* expression in Col WT and other genotypes including *sdg8*, *sdg7 sdg8*, *sdg8 mrg1 mrg2*, *OX-MRG2* and *sdg8 OX-MRG2* at 9 DAG only. (D, E) The interaction between MRG2 and histone H3 is dependent on H3K36me3. Schematic diagram for *in situ* PLA assay between MRG2 and histone H3 (D). *In situ* PLA assay using anti-HA and anti-H3 antibodies in *pMRG2::HA-MRG2* WT showed positive signals (upper panels in E), whilst *in situ* PLA assay with *pMRG2::HA-MRG2 sdg8* showed no signals (lower panels in E). Scale bar, 5  $\mu$ m. Blue, DAPI. Red, *in situ* PLA signals showing the interaction between HA-MRG2 and histone H3. Purple, merge.

tically reduced *FLC* expression was observed in *sdg7 sdg8* (Figure 4B) (47). Whilst *FLC* expression is reduced dramatically in *sdg8* mutant seedlings as well as in *sdg7 sdg8* at both DAG 6 and 9 (Figure 4B), the *FT* transcript is reduced to half at 9 DAG but not affected at 6 DAG in either *sdg8* or *sdg7 sdg8* (Figure 4C). These expression profiles of *FT* are similar to those observed in the *mrg1 mrg2* mutant (Figure 1E), suggesting that the SDG H3K36 methyltransferases and MRG proteins may function in the same pathway to regulate *FT*.

To test if the function of MRG1 and MRG2 requires H3K36 methylation, we performed genetic analyses. As the effects on *FLC* and *FT* in *sdg8* are as severe as those in *sdg7 sdg8*, we used the *sdg8* single mutant. In the *sdg8 mrg1 mrg2* triple mutant background, *FT* and *FLC* expression levels are similar to those in the *sdg8* single mutant (Figure 4B and C). This indicates that the function of *MRG1* and *MRG2* in flowering time control are dependent on *SDG8*-mediated H3K36me3. Overexpression of *MRG2* under the constitutive Cauliflower Mosaic Virus *p35S* promoter causes increased expression of *FLC* (~2 and 1.5-folds in 6 and 9 DAG, respectively) and decreased expression of *FT* at 9 DAG (~1.7-folds) (Figure 4B and C), leading to a late-flowering phenotype (Supplementary Figure S5). However, *35S::MRG2-HA* failed to affect the *FLC* transcript or flowering time in the *sdg8* mutant background (Figure 4B and Supplementary Figure S5), further confirming that the function of *MRG2* is dependent on *SDG8*. *FLC* reduction is more pronounced in *sdg8* than in *mrg1-1 mrg2-2* (Figures 1E and 4B), suggesting that H3K36me3 may have different effect in *FT* and *FLC* expression. It is possible that additional readers other than the MRG proteins, e.g. the PHD finger proteins, may prevent further down-regulation of *FLC* expression in *mrg1 mrg2* (48,49), and/or other H3K36me3-independent factors may maintain certain *FT* transcription level in *sdg8* and *mrg1 mrg2* (37,50–52).

Next, we tested whether the interaction of MRG proteins and histone H3 is dependent on H3K36me3 *in vivo*. We carried out the *in situ* PLA assay with antibodies for HA and histone H3 using *pMRG2::HA-MRG2* transgenic plants in the wild-type and *sdg8* mutant backgrounds. We observed positive signals that showed histone H3-MRG2 interaction in the wild-type background (Figure 4D and E). But the signals were abolished by the mutation of *sdg8* (Figure 4E), in which H3K36me3 is greatly decreased, whilst H3K4me3 and H3K36me2 are not changed or only moderately decreased (Figure 4A) (53,54), suggesting that MRG2 binding to histone H3 requires the H3K36me3 mark, whilst H3K4me3 and H3K36me2 are not sufficient to recruit MRG2 to histone H3 *in vivo*.

### MRG2 directly binds to *FT* genomic regions

*FT* expression is controlled by *CONSTANS* (CO) and several other genes, including some histone modifiers involved in the activation and repression along the light-dark phase change (55). We next examined how MRG1 or MRG2 regulates *FT* expression during LD conditions. Taking samples from the aerial part of seedlings at 9 DAG, we showed that *FT* expression in *mrg1 mrg2* is decreased to approximately

half at ZT 16 (the highest *FT* expression) and at most tested time points (Figure 5A). Interestingly, even at ZT 0 and ZT 24, at which the *FT* expression is at the lowest level during the entire light-dark cycle, the *FT* expression level in *mrg1 mrg2* is further reduced compared to WT (Figure 5A). In contrast, the *FT* expression level at 6 DAG did not show any obvious change between *mrg1 mrg2* and WT (Figure 1E). These results suggest that MRG1/2-mediated up-regulation may require pre-existing active transcription and the accumulation of the transcription-linked H3K36me3 mark to a certain level and that MRG1 and MRG2 may function continuously during the entire light-dark cycle once they have started.

To check if MRG2 directly regulates *FT* expression, we carried out ChIP assay with 9 DAG seedlings harvested at ZT16 and ZT24, in which *FT* expression is at the highest level and lowest level during the light-dark cycle, respectively. In both samples, the enrichment was detected in the regions of the promoter (*FT-P*) and exon 1 (*FT-E1*) but not in the region around intron 1 (*FT-I1*) (Figure 5B–D). Whilst the enrichment at ZT 16 is slightly higher than that ZT24, the difference is not so statistically significant. These results suggest that MRG2 directly binds to the *FT* locus throughout the day and night.

### MRG2 interacts with HATs to induce H4 acetylation

We next compared the histone acetylation levels of histone H3 (H3Ace) and histone H4K5 (H4K5Ace), and the activation marks of H3K4me3 and H3K36me3 between WT and *mrg1 mrg2* seedlings (Figure 6A–C, Supplementary Figure S6A–C). For ease of sampling, we harvested the seedlings at 10 DAG and tested the histone modification at the *FT* locus. Interestingly, whilst the levels of H3K36me3 were not obviously changed in *mrg1 mrg2* (Figure 6B), the H3K4me3 levels were clearly reduced in all tested primers at the promoter, exon 1 and intron 1 (Supplementary Figure S6B). Both the levels of H3Ace and H4K5Ace were decreased in *mrg1 mrg2* compared to WT at the regions around the promoter and exon 1, but not at the intron 1 of the *FT* locus (Figure 6C, Supplementary Figure S6C), suggesting that the function of *MRG1* and *MRG2* in *Arabidopsis* is mediated through histone acetylation, and possibly H3K4me3. When we compared the distribution patterns of these histone modifications, H3K36me3 and H4K5Ace levels were peaked at the exon 1, whilst H3Ace and H3K4me3 showed higher levels at the promoter (Figure 6D). Thus, we checked the possible interaction between MRG1/2 and MYST HATs, HAM1/2 proteins, that catalyse H4K5Ace (33,34). First, we carried out bimolecular fluorescence complementation (BiFC) assay by transiently co-expressing a translational fusion of MRG1/2 to the N-terminal portion of YFP (MRG1/2-nYFP) and fusion of HAM1/2 to the C-terminal portion of YFP (HAM1/2-cYFP) in tobacco. We were able to detect fluorescence signal in the nuclei of tobacco epidermal cells whilst the control (MRG1/2-nYFP and vector cYFP, vector nYFP and HAM1/2-cYFP) did not show any signals, suggesting that the observed BiFC between MRG1/2-nYFP and HAM1/2-cYFP are specific (Supplementary Figure S7). In addition, using a rabbit antibody against both HAM1 and HAM2, together with the

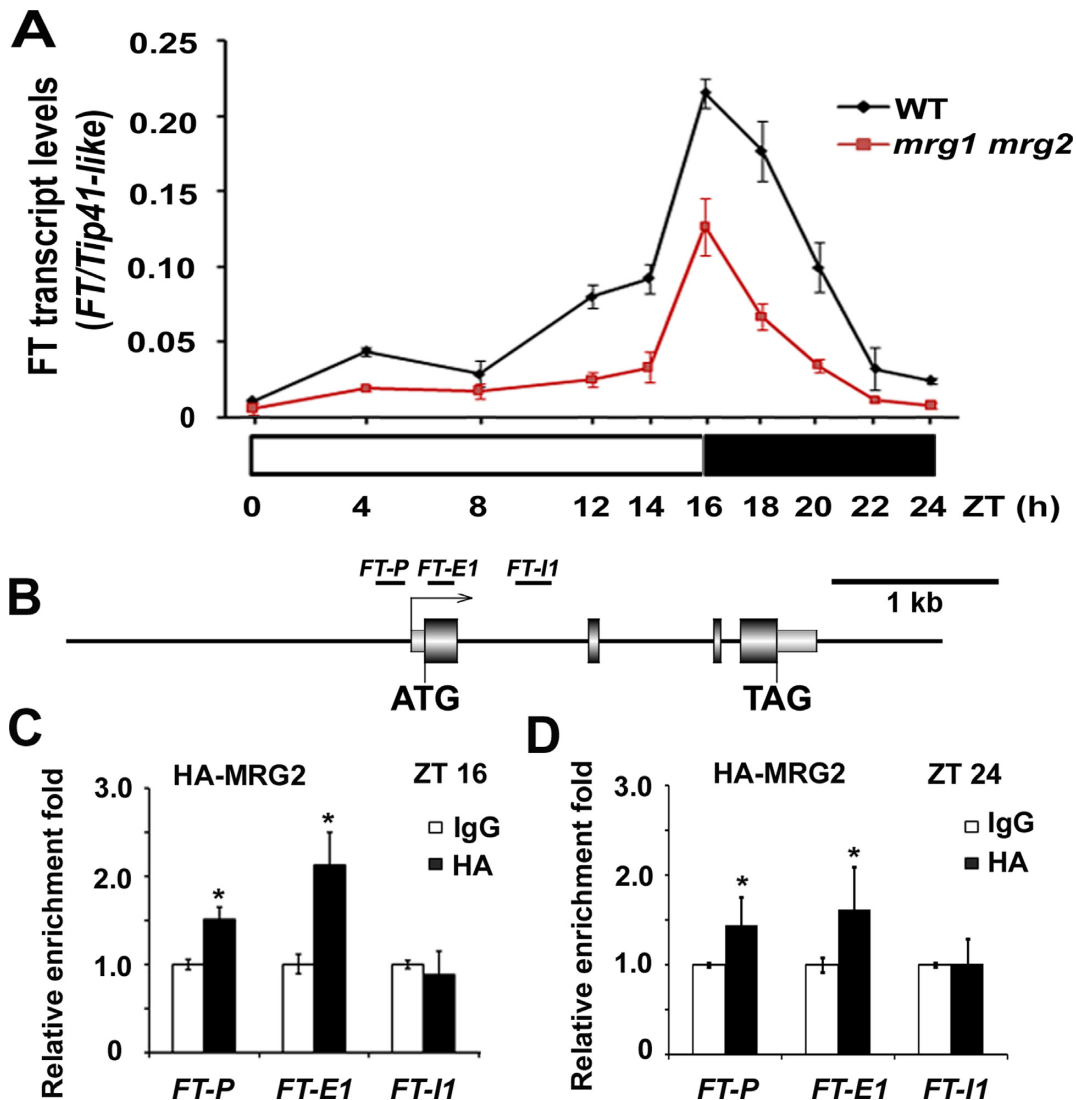


**Figure 5.** MRG2 binds directly to the *FT* locus. (A) *FT* mRNA levels in Col WT and *mrg1-1 mrg2-2* seedlings over a 24-h LD cycle. *FT* transcript levels were normalised to *Tip41-like*; bars indicate SD of triplicate measurements. White and dark bars below the x-axis indicate light and dark periods, respectively. One of two biological repeats with similar trends was shown. (B) Schematic drawing of the *FT* genome structure showing regions amplified by primers used for ChIP analysis. (C–D) ChIP analysis of HA-MRG2 enrichment at the *FT* locus at (C) ZT16 and (D) ZT24 with the *pMRG2::HA-MRG2* transgenic line. Amounts of the immunoprecipitated genomic fragments were measured by qPCR and normalised first to the endogenous control *ACTIN2* (*ACT2*). The fold enrichment of HA-MRG2 in each examined region was calculated by dividing the *ACT2*-normalised amount of the examined region from the sample with the anti-HA antibody by that with mouse IgG. Error bars indicate SD of six quantifications (three technical measurements of two biological replicates). \* $P < 0.05$  with Student's *t*-test.

mouse HA antibody against HA-MRG2, we performed an *in situ* PLA assay. We detected positive signals, further indicating the direct interaction between MRG2 and HAM1/2 (Figure 7A and B). Furthermore, we prepared and transformed the genomic DNA fusion construct of *HAM1* with HA inserted just after its ATG into *35S::GFP-MRG2* or wild-type plants. We performed Co-IP using the seedlings of *pHAM1::HA-HAM1 35S::GFP-MRG2*, with the seedling of *pHAM1::HA-HAM1* as the control. Indeed, anti-GFP antibody immunoprecipitated HA-HAM1 from the seedlings but not in the negative control with HA-HAM1 alone (Figure 7C). These results suggest that MRG proteins interact with HAM1/2 to induce histone H4 acety-

lation at the target loci that contained H3K36me3 (Figure 7D).

## DISCUSSION

In this study, we have shown that *Arabidopsis* *MRG15* homologues *MRG1* and *MRG2* function redundantly to stimulate the amplitude of expression of the flowering time genes *FT* and *FLC* in an H3K36me3-dependent manner. Due to the epistatic relationship between *FLC* and *FT*, the mutant shows late-flowering phenotype, caused by *FT* reduction.

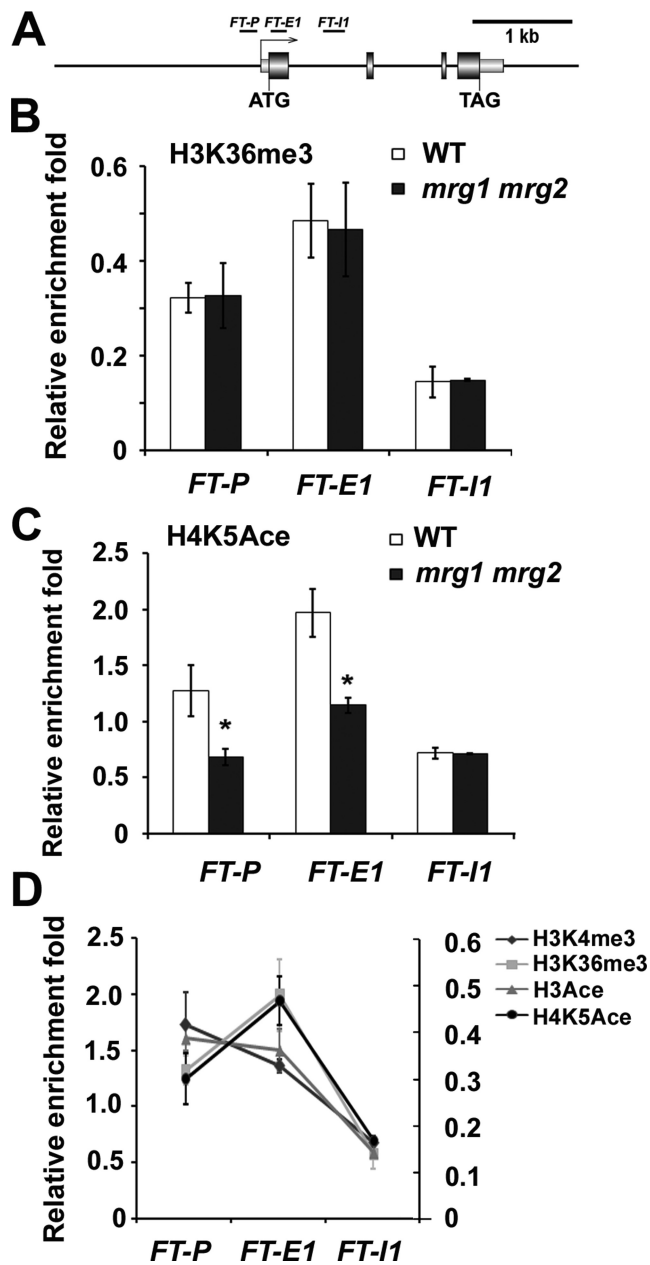


**Figure 6.** MRG1/2 maintain histone acetylation levels of the *FT* locus to ensure the high transcriptional level. (A) Schematic drawing of the *FT* genome structure showing regions amplified by primers used for ChIP analyses. (B, C) ChIP analyses of H3K36me3 (B), H4K5Ace (C). Enrichment at the *FT* locus in 10 DAG Col WT and *mrg1-1 mrg2-2* seedlings grown under LD 23°C. Amounts of the immunoprecipitated genomic fragments were measured by qPCR and normalised to the endogenous control *ACTIN2* (*ACT2*). White, WT; black, *mrg1 mrg2*. Bar indicates SD of six measurements (three measurements of two biological replicates) \* $P < 0.05$  with Student's *t*-test. (D) The distribution pattern of H3K4me3, H3K36me3, H3Ace and H4K5Ace in WT. Left Y-axis indicates relative enrichment fold of H3K4me3 and H4K5Ace, whilst right Y-axis indicates relative enrichment fold of H3K36me3 and H3Ace. It is based on the ChIP assays shown in B (for H3K36me3), C (for H4K5Ace) and Supplementary Figure S6B (for H3K4me3), S6C (for H3Ace).

### MRG1/2 bridges H3K36me3 and histone acetylation to achieve higher levels of flowering gene expression

Two flowering time genes, *FT* and *FLC*, with the opposing functions in floral transition, are down-regulated in mutant *mrg1 mrg2* (Figure 1E, Supplementary Figure S2F). It is not uncommon that one epigenetic regulation controls these two genes with opposing functions. For example, PRC2-like complex, including H3K27 methyltransferases CURLY LEAF (CLF) and SWINGER (SWN), deposits H3K27me3 at both *FLC* and *FT* to repress its expression (56,57). *FT* expression levels are similarly reduced in *sdg8*, *mrg1 mrg2* and *sdg8 mrg1 mrg2* at 9 DAG (Figures 1E and 4C), which support the idea that MRG proteins function in the same pathway as H3K36 methyltransferase SDG8. One paradox was why the *sdg8* mutant showed an early flowering phenotype (37) despite reduced expression of *FT* at 9 DAG. It could be caused by a significant reduction of *FLC* or increased *FT* expression at later time points. We found that *FT* was indeed increased at 12 DAG for an unknown reason (Supplementary Figure S8). Such up-regulation of the *FT* transcript appears to be independent of *MRG1/2* because the early flowering phenotype of *sdg8* is epistatic to the overexpression of *MRG2* (Supplementary Figure S5). Our other genetic data of *sdg8 mrg1 mrg2* also suggested that *sdg8* is epistatic to *mrg1 mrg2* in flowering control. These data do not contradict the model that MRG1 and MRG2 bind to SDG8-mediated-H3K36me3 and function through the mark to control downstream activities.

The *sdg8* mutation has different locus-specific effects on gene expression (54,58,59). Whilst the transcription of *FT* in 9 DAG is similarly impaired in *sdg8* and *mrg1 mrg2* mutant plants (Figures 1E and 4C), the *sdg8* mutation has a drastic effect on *FLC* expression compared with *mrg1 mrg2* mutation (Figures 1E and 4B). It is of note that H3K27me3 coexists with H3K4me3 at the 5'-end nucleosome of *FLC* (50). As H3K36me2/3 were reported to inhibit PcG-mediated repressive mark H3K27me3 (51,52), it is possible that the loss of H3K36me3 (Figure 4A), and also the dramatic reduction of H3K36me2 level at the *FLC* locus (37), lead to the spreading or increased level of H3K27me3 at the *FLC* region, thus greatly reducing *FLC* expression. However, it is interesting to note that *FT* chromatin also has a bivalent structure, simultaneously carrying the active H3K4me3 and repressive H3K27me3 marks (56,57). Thus, it is likely that the different levels of H3K4me3 on *FLC* and *FT* regions, which is also responsible to prevent H3K27me3 (51), determine the different effects of *sdg8* mutation on *FT* and *FLC* expression. This speculation requires further detailed study in the dynamic change of epigenetic mark in inducible rescue lines.

MRG proteins directly bind to HAM1/2 acetyltransferase and bridge the two histone modifications, H3K36me3 and H4 acetylation (Figures 6 and 7, Supplementary Figure S7). The *ham1 ham2* double mutant is not viable, and the single mutation of either *ham1* or *ham2* did not show any defects in the vegetative and reproductive stages (32). Interestingly, *ham1/+ ham2/+* and RNAi knockdown plants showed the reduction in *FLC* expression levels, as observed in *mrg1 mrg2*, and both overexpression of *HAM1* and *MRG2* caused late flowering phenotype with the increased

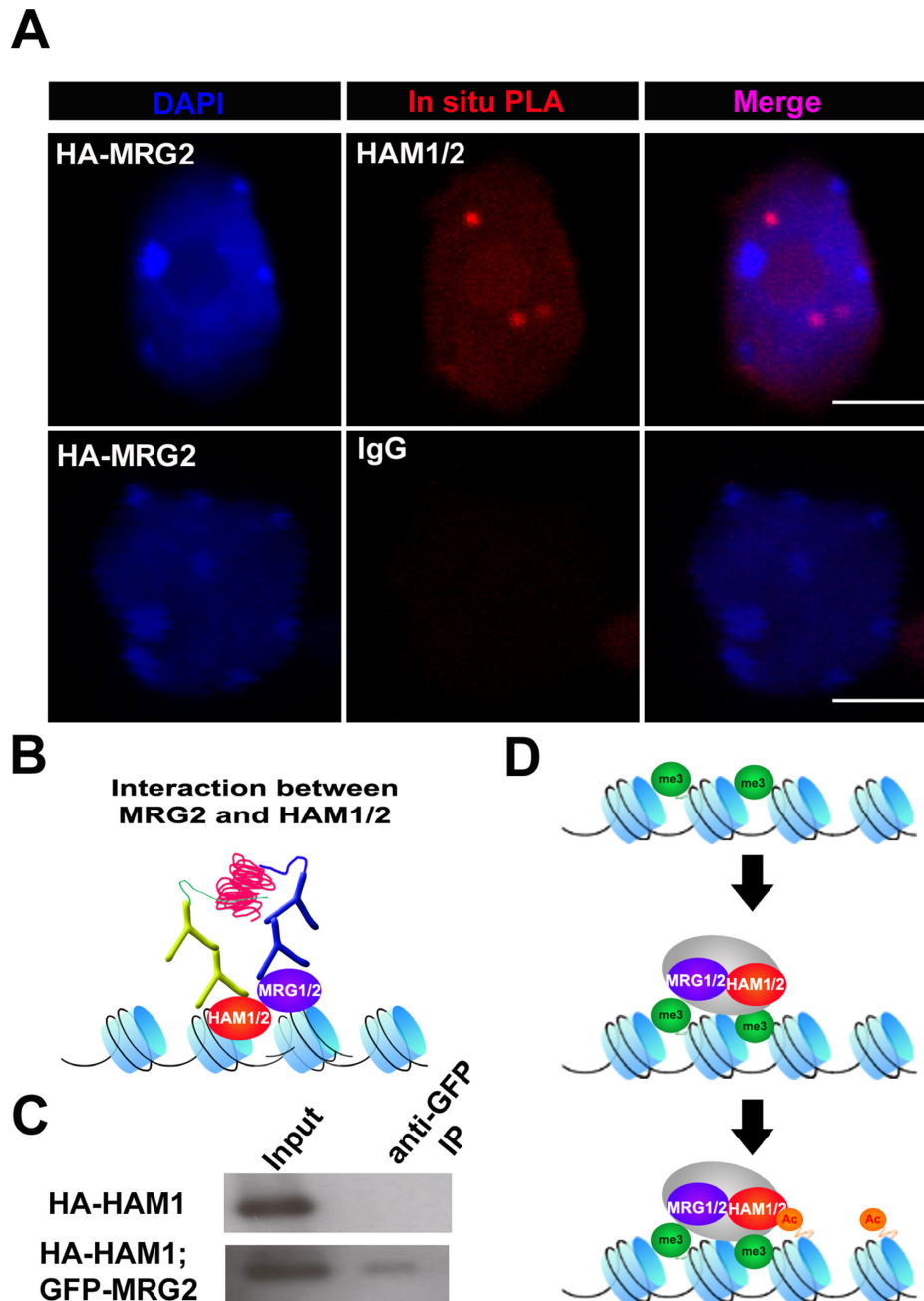


**Figure 7.** MRG1/2 recruits HAM1/2 to their targeted loci. (A) *In situ* PLA assay to show the interaction between MRG2 and HAM1/2. Blue, DAPI. Red, *in situ* PLA signal showing the interaction between HA-MRG2 and HAM1/2 (upper panels); the assay between HA-MRG2 and rabbit IgG was carried out as the negative control (lower panels). Purple, merge. Scale bar, 5  $\mu$ m. (B) Schematic diagram for *in situ* PLA assay between MRG2 and HAM1/2. (C) Co-IP assay to show the interaction between MRG2 and HAM1. Total protein extracted from 10 DAG seedlings co-expressing *HA-HAM1* and *GFP-MRG2* or solely expressing *HA-HAM1* (as the negative control), were subjected to immunoprecipitation with anti-GFP antibody. HA-HAM1 protein in the immunoprecipitates was detected by western blotting using anti-HA-HRP antibody. (D) A working model for the control of the target genes by MRG1/2 through the recruitment of HAM1/2-containing complex to increase the histone acetylation level at the target loci.

*FLC* transcription (Figures 1E and 4B and Supplementary Figure S5) (32,34). These results suggest that the MRG proteins and the HAM acetyltransferases function together to regulate *FLC*.

We showed that the approximately 2-fold reduction of *FT* expression is correlated with a reduced level of H4K5Ac at the 5' region of the *FT* locus in *mrg1 mrg2* seedlings (Figure 6C). In addition to H4K5Ac, we showed that the level of

H3Ac is also decreased at the *FT* locus in the *mrg1 mrg2* mutant (Supplementary Figure S6C). As MYST family proteins specifically catalyse histone H4 acetylation, H4K5Ac may help to recruit other histone acetyltransferases to amplify the effect of histone acetylation in different histones. The similar distribution pattern between H3K36me3 and H4K5Ac but not with H3Ac or H3K4me3 on the *FT* locus also indicates that the change of H4K5Ac level could

be the direct effect of *mrg1 mrg2* mutation (Figure 6A–D, Supplementary Figure S6A–C). Further experiments using the inducible line of *MRG1/2* in the *mrg1 mrg2* mutant could provide a suitable system to check the sequential steps of histone modifications.

*FT* expression is controlled by CO in a rhythmic pattern in LD conditions (55). Whilst several genes, including some histone modifiers, are required for the activation and repression of *FT* along the light-dark phase change. Newly identified *SAP30 FUNCTION-RELATED 1/2* (*AFR1/2*) only represses *FT* transcription at ZT 16, at the end of the light photoperiod (60). *FT* transcription is first detectable in seedlings at 4 DAG and dramatically increases at approximately 9–10 DAG during the floral transition (45). It is interesting to note that at 6 DAG, we were unable to detect a difference in *FT* transcription levels between the seedlings of WT and *mrg1 mrg2* plants suggesting MRG1/2 function is dispensable for *FT* expression at the early developmental stage (Figure 1E). Such a difference is only detectable at later stages such as 9 DAG (Figure 1E). This suggests that, upon reaching a certain developmental stage (between 6 and 9 DAG), MRG1 and MRG2 begin acting on the *FT* locus, which then on affect *FT* expression throughout the day and night (Figure 5), unlike *AFR1/2* which only regulates *FT* expression at ZT 16. MRG2 binding to H3K36me3 (Figure 3A–C) and the unaffected *FT* expression at 6 DAG suggest that the activating H3K36me3 epigenetic mark may need time to accumulate to recruit MRG1/2-containing complex to fine-tune transcription. The continuous binding of MRG2 to the *FT* locus during the light-dark cycle (Figure 5B–D) suggests that H3K36me3 is relatively stable throughout the day and night.

### Conservation and divergence of plant MRG protein functions

Similar to its homologous MRG15 proteins, *in vivo* and *in vitro* assays confirmed that MRG1 and MRG2 can bind to H3K36me3. The MRG15 family proteins are evolutionarily conserved in yeast and animals, and the chromodomains of MRG15 and Eaf3 bind to trimethylated H3K36 and H3K4 *in vitro* with a relatively weak affinity (2–4,14–16). Consistently, we found that the binding specificity of plant MRG15 homologues to H3K36me3 is also relatively conserved during evolution. An *in vitro* pull-down assay showed that the chromodomain of MRG1/2 directly binds to trimethylated H3K36 as well as H3K4me3, but the binding affinity is relatively weak (Figure 3A). Yeast Eaf3 has been reported to interact with other protein partners (e.g. PHD proteins) and shows a wide range of binding strength (from unstable to robust) to H3K36-methylated nucleosomes, which suggests that the combinatorial action of Eaf3 and PHD proteins strengthens the binding affinity (61). It is likely that other chromatin- or DNA-binding proteins also help MRG proteins in binding to their target loci with higher affinity *in vivo*. Alternatively, such weak affinity may allow MRG-containing complexes to spread histone acetylation across the target loci, as implicated in the dosage compensation complex (62).

Although the *in vitro* data showed that the chromodomain of MRG2 can bind to both H3K4me3 and H3K36me3 (Figure 3A), the *in situ* PLA assay suggested

that MRG2 binds to H3K36me3 specifically *in vivo* because the binding of MRG2 is completely abolished in the *sdg8* mutant, in which H3K36me3 is dramatically reduced, but H3K36me2 is still maintained albeit at a reduced level and H3K4me3 is intact (Figure 4A, D and E)(53,54). These data indicate that H3K36me3 is essential for MRG protein binding *in vivo*.

Whilst the human MRG15 and yeast Eaf3 are involved in both HATs and HDACs, most studies focus on the defects of its HDAC function because this effect is more obvious and the mutation effect is more severe (2–4,18–20). For example, in yeast, the deletion of *Eaf3* greatly alters the global genomic profile of histone acetylation, with increased acetylation levels at coding sequences and decreased acetylation levels at the promoter regions (21). However, these studies were rather focused on the function of Eaf3 binding to coding regions, recruiting an HDAC complex to H3K36me3-containing nucleosomes and thus prevents spurious intragenic transcription (2–4). Moreover, the loss of *Alp13*, the MRG15 homologue in fission yeast, causes global hyperacetylation of histones and chromosome instability (22). Thus, the function of MRG15 and its homologues associated with HATs was overlooked, partly because the loss of the MRG mutants causes phenotypes that are more linked with elevated histone acetylation on a gene-specific level or globally.

The interaction between MRG1/2 and MYST family proteins HAM1/2, characterised by an *in situ* PLA assay, BiFC assay and Co-IP analysis (Figure 7A–C, Supplementary Figure S7), confirmed the protein interaction between MRG1/2 and HATs. Whilst we could detect the interaction between MRG2 and HDA6 when transiently co-overexpressed in tobacco (Supplementary Figure S9), the resulting effects with the locus-specific decreased acetylation suggested that *MRG1* and *MRG2* could have diversified from its homologues in animal and yeast and primarily function in the fine-tuning of transcription regulation associated with HATs. It is possible that MRG1/2 proteins recruit both HAT and HDAC dynamically, and loss-of-function of *mrg1 mrg2* leads to the disruption of a balance between these two counteracting activities, resulting in the reduction of histone acetylation levels and transcription. In human T cells, genome-wide mapping of HATs and HDACs binding showed that regions enriched with both HATs and HDACs are linked with active genes (63). They showed that in both active genes and primed genes (genes poised for expression later), inhibition of HDAC activity causes increased acetylation level at the promoter regions (63), rather than the reduced acetylation level we observed in *mrg1 mrg2* (Figure 6C, Supplementary Figure S6C). In addition, at active gene loci, HDAC physically interacts with the elongating form of RNA Pol II and is directly recruited to actively transcribed regions by RNA Pol II, which may bypass the need for H3K36me3 (63). Moreover, the histone deacetylase HDA6 in *Arabidopsis* is recruited to remove acetylated histone marks at the *FT* locus specifically at dusk under long-day conditions, thereby dampening *FT* mRNA expression after its transcriptional activation by CO. Mutation of the HDAC recruiter increases the histone acetylation level at the *FT* locus (60). As perturbation of HDAC generally leads to increased histone acetylation levels, the opposite effect of

the reduction of histone acetylation level at the *FT* locus in *mrg1 mrg2* mutant suggests that the function of MRG1/2 on *FT* is majorly dependent on its interaction with HATs.

The loss-of-function of *MRG1* and *MRG2* causes an approximately 2-fold decrease in the expression levels, together with the reduction of the histone acetylation levels at their target genes. It can be argued that the decreased *FT* expression is due to the decreased H3K4me3 and H3Ace. Although we have shown that H3K36me3 is essential for MRG2 binding to chromatin (Figure 4E), it is still possible that H3K4me3 is also necessary for MRG2-dependent expression of *FT*, as transcriptional regulation is mediated by complex cross-talk of multiple histone modifications. However, based on our results that MRG1/2 can form complex with the HATs specific for H4, HAM1/2, *in vitro* and *in vivo* (Figure 7 and Supplementary Figure S7) and co-localisation between H3K36me3 and H4 acetylation at the promoter region (Figure 6D), we favour the hypothesis that the binding of MRG proteins to H3K36me3 leads to the H4 acetylation for transcriptional induction and that the reduction of H3K4me3 and H3Ace levels in *mrg1 mrg2* could be the secondary effects of transcription reduction. This suggests that the MRG1/2 functions resemble the dosage compensation complex in *Drosophila* that contains MSL3 (MRG protein not belonging to the MRG15 subfamily) and MOF (MYST family HAT) (64,65). The binding of MRG2 to H3K36me3 at the target loci could facilitate the spread of histone acetylation through the recruitment of the MRG2-containing HAT complex, in a similar manner as the MSL3-containing dosage compensation complex (64,65).

In *Arabidopsis*, H3K36me3 co-localises with other activation marks, including H3K4me3 and H3K56Ace, at the active chromatin (6). This simultaneous occurrence of multiple epigenetic marks has no equivalent in *Drosophila*, *C. elegans* and humans (6). Moreover, in *Arabidopsis*, H3K36me3 peaks in the 5'-end of the coding region, which is in contrast to the 3'-end enrichment in other organisms (6). MRG1 and MRG2 may be involved in the association of H3K36me3 and histone acetylation marks. Indeed, at the *FT* locus, H4K5Ace distribution pattern is similar to that of H3K36me3 peaking at the 5'-end of the coding region (Figure 6D). Such a difference of the distribution pattern of H3K36me3 between plants and other organisms may be a result of co-evolution with the functional diversification of MRG15 proteins.

## SUPPLEMENTARY DATA

Supplementary Data are available at NAR Online.

## ACKNOWLEDGEMENT

We thank Aiwu Dong for communication on the *mrg2-1* mutant and for research discussion.

*Author Contributions.* T.I. conceived of the study, supervised and coordinated the study. Y.X., E.-S.G. J.Z. and T.I. designed the experiments. Y.X., E.-S.G. and W.-Y.W. performed the ChIP experiments, immunolocalisation analysis, *in situ* PLA assays and the microarray studies. Y.X., J.Z. and W.-Y.W. performed the genetic analysis. Y.X. and T.I. wrote the manuscript. All authors discussed the results and approved the final manuscript.

## FUNDING

Temasek Life Sciences Laboratory (TLL) [to T.I.]; National Research Foundation Singapore under its Competitive Research Program [CRP Award No. NRF-CRP001-108].

*Conflict of interest statement.* None declared.

## REFERENCES

- Kolasinska-Zwierz, P., Down, T., Latorre, I., Liu, T., Liu, X.S. and Ahringer, J. (2009) Differential chromatin marking of introns and expressed exons by H3K36me3. *Nat. Genet.*, **41**, 376–381.
- Carrozza, M.J., Li, B., Florens, L., Suganuma, T., Swanson, S.K., Lee, K.K., Shia, W.J., Anderson, S., Yates, J., Washburn, M.P. *et al.* (2005) Histone H3 methylation by Set2 directs deacetylation of coding regions by Rpd3S to suppress spurious intragenic transcription. *Cell*, **123**, 581–592.
- Joshi, A.A. and Struhl, K. (2005) Eaf3 chromodomain interaction with methylated H3-K36 links histone deacetylation to Pol II elongation. *Mol. Cell*, **20**, 971–978.
- Keogh, M.C., Kurdastani, S.K., Morris, S.A., Ahn, S.H., Podolny, V., Collins, S.R., Schuldiner, M., Chin, K., Punna, T., Thompson, N.J. *et al.* (2005) Cotranscriptional set2 methylation of histone H3 lysine 36 recruits a repressive Rpd3 complex. *Cell*, **123**, 593–605.
- Luco, R.F., Pan, Q., Tominaga, K., Blencowe, B.J., Pereira-Smith, O.M. and Misteli, T. (2010) Regulation of alternative splicing by histone modifications. *Science*, **327**, 996–1000.
- Roudier, F., Ahmed, I., Berard, C., Sarazin, A., Mary-Huard, T., Cortijo, S., Bouyer, D., Caillieux, E., Duvernois-Berthet, E., Al-Shikhley, L. *et al.* (2011) Integrative epigenomic mapping defines four main chromatin states in Arabidopsis. *EMBO J.*, **30**, 1928–1938.
- Marin, I. and Baker, B.S. (2000) Origin and evolution of the regulatory gene male-specific lethal-3. *Mol. Biol. Evol.*, **17**, 1240–1250.
- Bertram, M.J. and Pereira-Smith, O.M. (2001) Conservation of the MORF4 related gene family: identification of a new chromo domain subfamily and novel protein motif. *Gene*, **266**, 111–121.
- Berger, S.L. (2007) The complex language of chromatin regulation during transcription. *Nature*, **447**, 407–412.
- Jacobs, S.A. and Khorasanizadeh, S. (2002) Structure of HP1 chromodomain bound to a lysine 9-methylated histone H3 tail. *Science*, **295**, 2080–2083.
- Nielsen, P.R., Nietlispach, D., Mott, H.R., Callaghan, J., Bannister, A., Kouzarides, T., Murzin, A.G., Murzina, N.V. and Laue, E.D. (2002) Structure of the HP1 chromodomain bound to histone H3 methylated at lysine 9. *Nature*, **416**, 103–107.
- Min, J., Zhang, Y. and Xu, R.M. (2003) Structural basis for specific binding of Polycomb chromodomain to histone H3 methylated at Lys 27. *Genes Dev.*, **17**, 1823–1828.
- Fischle, W., Wang, Y., Jacobs, S.A., Kim, Y., Allis, C.D. and Khorasanizadeh, S. (2003) Molecular basis for the discrimination of repressive methyl-lysine marks in histone H3 by Polycomb and HP1 chromodomains. *Genes Dev.*, **17**, 1870–1881.
- Sun, B., Hong, J., Zhang, P., Dong, X., Shen, X., Lin, D. and Ding, J. (2008) Molecular basis of the interaction of *Saccharomyces cerevisiae* Eaf3 chromo domain with methylated H3K36. *J. Biol. Chem.*, **283**, 36504–36512.
- Xu, C., Cui, G., Botuyan, M.V. and Mer, G. (2008) Structural basis for the recognition of methylated histone H3K36 by the Eaf3 subunit of histone deacetylase complex Rpd3S. *Structure*, **16**, 1740–1750.
- Zhang, P., Du, J., Sun, B., Dong, X., Xu, G., Zhou, J., Huang, Q., Liu, Q., Hao, Q. and Ding, J. (2006) Structure of human MRG15 chromo domain and its binding to Lys36-methylated histone H3. *Nucleic Acids Res.*, **34**, 6621–6628.
- Leung, J.K., Berube, N., Venable, S., Ahmed, S., Timchenko, N. and Pereira-Smith, O.M. (2001) MRG15 activates the B-myb promoter through formation of a nuclear complex with the retinoblastoma protein and the novel protein PAM14. *J. Biol. Chem.*, **276**, 39171–39178.
- Pardo, P.S., Leung, J.K., Lucchesi, J.C. and Pereira-Smith, O.M. (2002) MRG15, a novel chromodomain protein, is present in two distinct multiprotein complexes involved in transcriptional activation. *J. Biol. Chem.*, **277**, 50860–50866.

19. Allard,S., Utlej,R.T., Savard,J., Clarke,A., Grant,P., Brandl,C.J., Pillus,L., Workman,J.L. and Cote,J. (1999) NuA4, an essential transcription adaptor/histone H4 acetyltransferase complex containing Esa1p and the ATM-related cofactor Tra1p. *EMBO J.*, **18**, 5108–5119.
20. Eisen,A., Utlej,R.T., Nourani,A., Allard,S., Schmidt,P., Lane,W.S., Lucchesi,J.C. and Cote,J. (2001) The yeast NuA4 and Drosophila MSL complexes contain homologous subunits important for transcription regulation. *J. Biol. Chem.*, **276**, 3484–3491.
21. Reid,J.L., Moqtaderi,Z. and Struhl,K. (2004) Eaf3 regulates the global pattern of histone acetylation in *Saccharomyces cerevisiae*. *Mol. Cell. Biol.*, **24**, 757–764.
22. Nakayama,J., Xiao,G., Noma,K., Malikzay,A., Bjerling,P., Ekwall,K., Kobayashi,R. and Grewal,S.I. (2003) Alp13, an MRG family protein, is a component of fission yeast Clr6 histone deacetylase required for genomic integrity. *EMBO J.*, **22**, 2776–2787.
23. Chen,E.S., Zhang,K., Nicolas,E., Cam,H.P., Zofall,M. and Grewal,S.I. (2008) Cell cycle control of centromeric repeat transcription and heterochromatin assembly. *Nature*, **451**, 734–737.
24. Reid,J.L., Iyer,V.R., Brown,P.O. and Struhl,K. (2000) Coordinate regulation of yeast ribosomal protein genes is associated with targeted recruitment of Esa1 histone acetylase. *Mol. Cell*, **6**, 1297–1307.
25. Vogelauer,M., Wu,J., Suka,N. and Grunstein,M. (2000) Global histone acetylation and deacetylation in yeast. *Nature*, **408**, 495–498.
26. Boudreault,A.A., Cronier,D., Selleck,W., Lacoste,N., Utlej,R.T., Allard,S., Savard,J., Lane,W.S., Tan,S. and Cote,J. (2003) Yeast enhancer of polycomb defines global Esa1-dependent acetylation of chromatin. *Genes Dev.*, **17**, 1415–1428.
27. Dombecki,C.R., Chiang,A.C., Kang,H.J., Bilgir,C., Stefanski,N.A., Neva,B.J., Klerkx,E.P. and Nabeshima,K. (2011) The chromodomain protein MRG-1 facilitates SC-independent homologous pairing during meiosis in *Caenorhabditis elegans*. *Dev. Cell*, **21**, 1092–1103.
28. Lusser,A., Kolle,D. and Loidl,P. (2001) Histone acetylation: lessons from the plant kingdom. *Trends Plant Sci.*, **6**, 59–65.
29. Carrozza,M.J., Utlej,R.T., Workman,J.L. and Cote,J. (2003) The diverse functions of histone acetyltransferase complexes. *Trends Genet.*, **19**, 321–329.
30. Smith,E.R., Pannuti,A., Gu,W., Steurnagel,A., Cook,R.G., Allis,C.D. and Lucchesi,J.C. (2000) The drosophila MSL complex acetylates histone H4 at lysine 16, a chromatin modification linked to dosage compensation. *Mol. Cell. Biol.*, **20**, 312–318.
31. Conrad,T., Cavalli,F.M., Holz,H., Hallaceli,E., Kind,J., Ilik,I., Vaquerizas,J.M., Luscombe,N.M. and Akhtar,A. (2012) The MOF chromobarrel domain controls genome-wide H4K16 acetylation and spreading of the MSL complex. *Dev. Cell*, **22**, 610–624.
32. Latrassé,D., Benhamed,M., Henry,Y., Domenichini,S., Kim,W., Zhou,D.X. and Delarue,M. (2008) The MYST histone acetyltransferases are essential for gametophyte development in *Arabidopsis*. *BMC Plant Biol.*, **8**, 121.
33. Earley,K.W., Shook,M.S., Brower-Toland,B., Hicks,L. and Pikaard,C.S. (2007) In vitro specificities of *Arabidopsis* co-activator histone acetyltransferases: implications for histone hyperacetylation in gene activation. *Plant J.*, **52**, 615–626.
34. Xiao,J., Zhang,H., Xing,L., Xu,S., Liu,H., Chong,K. and Xu,Y. (2013) Requirement of histone acetyltransferases HAM1 and HAM2 for epigenetic modification of FLC in regulating flowering in *Arabidopsis*. *J. Plant Physiol.*, **170**, 444–451.
35. He,Y. (2012) Chromatin regulation of flowering. *Trends Plant Sci.*, **17**, 556–562.
36. Strahl,B.D., Grant,P.A., Briggs,S.D., Sun,Z.W., Bone,J.R., Caldwell,J.A., Mollah,S., Cook,R.G., Shabanowitz,J., Hunt,D.F. *et al.* (2002) Set2 is a nucleosomal histone H3-selective methyltransferase that mediates transcriptional repression. *Mol. Cell. Biol.*, **22**, 1298–1306.
37. Zhao,Z., Yu,Y., Meyer,D., Wu,C. and Shen,W.H. (2005) Prevention of early flowering by expression of FLOWERING LOCUS C requires methylation of histone H3 K36. *Nat. Cell Biol.*, **7**, 1256–1260.
38. Grini,P.E., Thorstensen,T., Alm,V., Vizcay-Barrena,G., Windju,S.S., Jorstad,T.S., Wilson,Z.A. and Aalen,R.B. (2009) The ASH1 HOMOLOG 2 (ASHH2) histone H3 methyltransferase is required for ovule and anther development in *Arabidopsis*. *PLoS One*, **4**, e7817.
39. Czechowski,T., Stitt,M., Altmann,T., Udvardi,M.K. and Scheible,W.R. (2005) Genome-wide identification and testing of superior reference genes for transcript normalization in *Arabidopsis*. *Plant Physiol.*, **139**, 5–17.
40. Sun,B., Xu,Y., Ng,K.H. and Ito,T. (2009) A timing mechanism for stem cell maintenance and differentiation in the *Arabidopsis* floral meristem. *Genes Dev.*, **23**, 1791–1804.
41. Xu,Y., Wang,Y., Stroud,H., Gu,X., Sun,B., Gan,E.S., Ng,K.H., Jacobsen,S.E., He,Y. and Ito,T. (2013) A matrix protein silences transposons and repeats through interaction with retinoblastoma-associated proteins. *Curr. Biol.*, **23**, 345–350.
42. Lee,L.Y., Fang,M.J., Kuang,L.Y. and Gelvin,S.B. (2008) Vectors for multi-color bimolecular fluorescence complementation to investigate protein-protein interactions in living plant cells. *Plant Methods*, **4**, 24.
43. Sparkes,I.A., Runions,J., Kearns,A. and Hawes,C. (2006) Rapid, transient expression of fluorescent fusion proteins in tobacco plants and generation of stably transformed plants. *Nat. Protoc.*, **1**, 2019–2025.
44. Lysak,M., Frasz,P. and Schubert,I. (2006) Cytogenetic analyses of *Arabidopsis*. *Methods Mol. Biol.*, **323**, 173–186.
45. Kobayashi,Y., Kaya,H., Goto,K., Iwabuchi,M. and Araki,T. (1999) A pair of related genes with antagonistic roles in mediating flowering signals. *Science*, **286**, 1960–1962.
46. Koos,B., Andersson,L., Clauson,C.M., Grannas,K., Klaesson,A., Cane,G. and Soderberg,O. (2014) Analysis of protein interactions in situ by proximity ligation assays. *Curr. Top. Microbiol. Immunol.*, **377**, 111–126.
47. Bell,O., Wirbelauer,C., Hild,M., Scharf,A.N., Schwaiger,M., MacAlpine,D.M., Zilbermann,F., van Leeuwen,F., Bell,S.P., Imhof,A. *et al.* (2007) Localized H3K36 methylation states define histone H4K16 acetylation during transcriptional elongation in *Drosophila*. *EMBO J.*, **26**, 4974–4984.
48. Musselman,C.A., Avvakumov,N., Watanabe,R., Abraham,C.G., Lalonde,M.E., Hong,Z., Allen,C., Roy,S., Nunez,J.K., Nickloff,J. *et al.* (2012) Molecular basis for H3K36me3 recognition by the Tudor domain of PHF1. *Nat. Struct. Mol. Biol.*, **19**, 1266–1272.
49. Vezzoli,A., Bonadies,N., Allen,M.D., Freund,S.M., Santiveri,C.M., Kvinlaug,B.T., Huntly,B.J., Gottgens,B. and Bycroft,M. (2010) Molecular basis of histone H3K36me3 recognition by the PWWP domain of Brpf1. *Nat. Struct. Mol. Biol.*, **17**, 617–619.
50. Saleh,A., Alvarez-Venegas,R. and Avramova,Z. (2008) Dynamic and stable histone H3 methylation patterns at the *Arabidopsis* FLC and AP1 loci. *Gene*, **423**, 43–47.
51. Schmitges,F.W., Prusty,A.B., Faty,M., Stutzer,A., Lingaraju,G.M., Aiwazian,J., Sack,R., Hess,D., Li,L., Zhou,S. *et al.* (2011) Histone methylation by PRC2 is inhibited by active chromatin marks. *Mol. Cell*, **42**, 330–341.
52. Yuan,W., Xu,M., Huang,C., Liu,N., Chen,S. and Zhu,B. (2011) H3K36 methylation antagonizes PRC2-mediated H3K27 methylation. *The Journal of biological chemistry*, **286**, 7983–7989.
53. Xu,L., Zhao,Z., Dong,A., Soubigou-Taconnat,L., Renou,J.P., Steinmetz,A. and Shen,W.H. (2008) Di- and tri- but not monomethylation on histone H3 lysine 36 marks active transcription of genes involved in flowering time regulation and other processes in *Arabidopsis thaliana*. *Mol. Cell. Biol.*, **28**, 1348–1360.
54. Palma,K., Thorgrimsen,S., Malinovsky,F.G., Fiil,B.K., Nielsen,H.B., Brodersen,P., Hofius,D., Petersen,M. and Mundy,J. (2010) Autoimmunity in *Arabidopsis* acd11 is mediated by epigenetic regulation of an immune receptor. *PLoS Pathog.*, **6**, e1001137.
55. Suarez-Lopez,P., Wheatley,K., Robson,F., Onouchi,H., Valverde,F. and Coupland,G. (2001) CONSTANS mediates between the circadian clock and the control of flowering in *Arabidopsis*. *Nature*, **410**, 1116–1120.
56. Jiang,D., Wang,Y. and He,Y. (2008) Repression of FLOWERING LOCUS C and FLOWERING LOCUS T by the *Arabidopsis* Polycomb repressive complex 2 components. *PLoS One*, **3**, e3404.
57. Oh,S., Park,S. and van Nocker,S. (2008) Genic and global functions for Paf1C in chromatin modification and gene expression in *Arabidopsis*. *PLoS Genet.*, **4**, e1000077.
58. Cazzonelli,C.I., Roberts,A.C., Carmody,M.E. and Pogson,B.J. (2010) Transcriptional control of SET DOMAIN GROUP 8 and CAROTENOID ISOMERASE during *Arabidopsis* development. *Mol. Plant*, **3**, 174–191.
59. Cazzonelli,C.I., Cuttriss,A.J., Cossetto,S.B., Pye,W., Crisp,P., Whelan,J., Finnegan,E.J., Turnbull,C. and Pogson,B.J. (2009)

- Regulation of carotenoid composition and shoot branching in Arabidopsis by a chromatin modifying histone methyltransferase, SDG8. *Plant Cell*, **21**, 39–53.
60. Gu, X., Wang, Y. and He, Y. (2013) Photoperiodic regulation of flowering time through periodic histone deacetylation of the florigen gene FT. *PLoS Biol.*, **11**, e1001649.
61. Li, B., Gogol, M., Carey, M., Lee, D., Seidel, C. and Workman, J.L. (2007) Combined action of PHD and chromo domains directs the Rpd3S HDAC to transcribed chromatin. *Science*, **316**, 1050–1054.
62. Gelbart, M.E., Larschan, E., Peng, S., Park, P.J. and Kuroda, M.I. (2009) Drosophila MSL complex globally acetylates H4K16 on the male X chromosome for dosage compensation. *Nat. Struct. Mol. Biol.*, **16**, 825–832.
63. Wang, Z., Zang, C., Cui, K., Schones, D.E., Barski, A., Peng, W. and Zhao, K. (2009) Genome-wide mapping of HATs and HDACs reveals distinct functions in active and inactive genes. *Cell*, **138**, 1019–1031.
64. Morales, V., Regnard, C., Izzo, A., Vetter, I. and Becker, P.B. (2005) The MRG domain mediates the functional integration of MSL3 into the dosage compensation complex. *Mol. Cell. Biol.*, **25**, 5947–5954.
65. Bell, O., Conrad, T., Kind, J., Wirbelauer, C., Akhtar, A. and Schubeler, D. (2008) Transcription-coupled methylation of histone H3 at lysine 36 regulates dosage compensation by enhancing recruitment of the MSL complex in *Drosophila melanogaster*. *Mol. Cell. Biol.*, **28**, 3401–3409.